Journal of Petroleum Science and Engineering 122 (2014) 31–37

Contents lists available at ScienceDirect

Journal of Petroleum Science and Engineering

journal homepage: www.elsevier.com/locate/petrol

Effects of acid–rock reaction heat on fluid temperature profile in fracture during acid fracturing in carbonate reservoirs

Jianchun Guo [a,*], Huifeng Liu [b], Yuanqiang Zhu [c], Yuxuan Liu [a]

[a] State Key Laboratory of Oil and Gas Reservoir Geology and Exploitation, Southwest Petroleum University, Chengdu 610500, China
[b] Research Institute of Oil and Gas Engineering, Tarim Oil Field Company, Petrochina, Xinjiang 841000, China
[c] School of Chemistry and Chemical Engineering, Southwest Petroleum University, Chengdu 610500, China

ARTICLE INFO

Article history:
Received 12 May 2012
Accepted 13 August 2014
Available online 29 August 2014

Keywords:
acid–rock reaction heat
coupling
volumetric work
PKN fracture model

ABSTRACT

During acid fracturing, the acid–rock reaction heat changes significantly with temperature, acid concentration and pressure. The variance of acid–rock reaction heat will change the temperature profile in the fracture, and consequently affect the effective fracture geometry created by the acid. With consideration of the effects of temperature, pressure and volumetric work of CO_2 produced by reaction, a method coupling the acid–rock reaction heat with a 2-dimension model of the fluid temperature profile along a fracture has been studied to develop a model for calculating the fluid temperature profiles applicable for acid fracturing of carbonate reservoirs. The analysis results show that acid–rock reaction heat can cause a maximum temperature increase of about 15 °C to fracture fluid. It was further observed that the effect of acid–rock reaction heat on temperature profiles is more pronounced by using higher acid concentrations in low temperature formation. Our method shows the significance of including the acid–rock reaction heat in the fracture to achieve a more accurate calculation of the fracture temperature profile in acid fracturing wells.

1. Introduction

Acid fracturing is a common method used to stimulate carbonate reservoirs. The etched fracture geometry created by the acid is an important parameter used to evaluate the impact of the stimulation. Simulations from acid fracturing model (Settari, 1993) have indicated that temperature profile is of great importance in simulating the acidizing process, and heat of reaction is one of the key parameters determining the temperature profile.

Calculation of temperature profile contains two parts, in the wellbore and in the reservoir. The first problem has been widely investigated (Squier et al., 1962; Wu and Pruess, 1990; Hasan and Kabir, 1994). While the second problem is more complicated, it involves the effect of chemical reaction in acid fracturing. Many researchers have focused on the problem concerning temperature distribution in the etched channel. Dysart and Whitsitt (1967) focused on the problem of fluid temperature prediction in fractures.

Then Whitsitt and Dysart (1970) derived an improved representative thermal model, which is an analytical expression for heat transfer from formation rocks to fracture fluids. Their model is a simple description of the temperature profile in simulation, which does not consider the reaction heat emerging only in acidizing. After that, Lee and Roberts (1980) considered acid–rock reaction heat as a boundary condition of the temperature profile model. However, the reaction heat in their model is a constant, not a variable depending on the chemical reaction heat. Ren and Xiong (1989) developed a new mathematical model for the reaction of acid flowing in the fracture, which considers the common ion effect in acid/rock reaction heat. Zhu and Hill (1991) presented a mathematical and numerical model to simulate temperature and pressure behavior during a mini-frac test. They calculated the heat exchange between fracture fluids and formation rocks using different methods, but did not consider the reaction heat. Roodhart et al. (1993) developed a numerical simulator for the calculation of the temperature profile, adding an item describing acid–rock reaction heat to the energy conservation equation. Medeiros Jr. and Trevisan (2006) addressed the heat transfer in the formation during acid treatments. They included the reaction heat in their numerical model and successfully predicted the temperature in the formation.

The reaction heat is not a constant as treated in some papers (Lee and Roberts, 1980). It depends on the temperature and pressure in the fracture and can be calculated through the enthalpies of reactants and resultants, as in Medeiros Jr. and Trevisan (2006). In this paper, we developed a new model for calculating the acid/rock reaction heat, considering the effects of temperature, pressure and volumetric work of CO_2 in acid–rock molar reaction heat. Then models of acid–rock reaction heat and fluid temperature profile are coupled and solved together. The model and method described in this paper

* Corresponding author.
E-mail address: guojianchun@vip.163.com (J. Guo).

http://dx.doi.org/10.1016/j.petrol.2014.08.016
0920-4105/

Nomenclature

C	leak-off coefficient of acid ($m\ min^{-0.5}$)
C_A	acid concentration ($mol\ L^{-1}$)
C_{A0}	initial acid concentration ($mol\ L^{-1}$)
$C_{p,m}$	constant-pressure molar heat capacity ($J\ K^{-1}\ mol^{-1}$)
C_f	specific heat of fracture fluid ($J\ kg^{-1}\ ^\circ C^{-1}$)
C_w	acid concentration at fracture surface ($mol\ L^{-1}$)
$\overline{C_A}$	average values of acid concentration in the direction of the fracture width (mol/L)
E	Young's modulus (MPa)
f_g	the molar fraction of free CO_2
h	thickness of the formation (m)
h_T	heat transfer coefficient ($W\ m^{-2}\ ^\circ C^{-1}$)
K_{hf}	thermal conductivity of fracture fluid ($W\ m^{-1}\ ^\circ C^{-1}$)
k_R	reaction rate constant ($((mol\ L^{-1})^{-m}\cdot(mol\ cm^{-2}\ s^{-1}))$)
k_g	mass transfer coefficient ($m\ s^{-1}$)
L	fracture length (m)
m	the order of reaction
p	pressure (MPa)
P_c	closure pressure (MPa)
Q_i	injection rate ($m^3\ min^{-1}$)
$q_h(t)$	heat flux from the formation to fracture ($J\ m^{-0.5}\ s^{-0.5}$)
S_{CO_2}	solution of CO_2 in reacted acid at certain temperature and pressure ($m^3\ m^3$)
t	time (min)
T_0	initial temperature
T_w	temperature at fracture surface (K)
$\overline{T}$	average values of acid temperature in the direction of the fracture width (°C)
ν	Poisson's ratio
ν_i	stoichiometric coefficient of substance i in the chemical reaction equation
V_i	molar volume of i, ($m^3\ mol^{-1}$)
V_{CO_2}	molar volume of CO_2 ($m^3\ mol^{-1}$)
V_{acid}	volume of the reacted acid (L)
ν_x	flow velocity of acid in the direction of fracture length ($m\ s^{-1}$)
ν_y	flow velocity of acid in the direction of fracture width ($m\ s^{-1}$)
ν_l	leak off velocity ($m\ s^{-1}$)
$\overline{v_x}$	average values of velocity in the direction of the fracture width ($m\ s^{-1}$)
w	average fracture width along the fracture height (m)
x	distance from wellbore (m)

Greeks

$\Delta_r H_m^\Theta$	molar reaction enthalpy ($kJ\ mol^{-1}$)
$\Delta_f H_m^\Theta$	standard molar formation enthalpies ($kJ\ mol^{-1}$)
$\Delta_r Q_m(T_w, p)$	molar reaction heat of reacting calcium carbonate and hydrochloric acid ($kJ\ mol^{-1}$)
μ_f	fluid viscosity (mPa s)
ρ_f	density of fracture fluid ($g\ cm^{-3}$)

Conversion factors for metric SI

$1\ ^\circ C - 272.15 = 1\ K$
$MPa \times 1E-06 = 1\ Pa$
$1\ m^3\ min^{-1} \times 60 = 1\ m^3\ s^{-1}$
$1\ mPa\ s \times 1E+03 = 1\ Pa\ s$
$1\ W = 1\ J\ s^{-1}$
$1\ cm^2 \times 1E+04 = 1\ m^2$
$1\ g\ cm^{-3} \times 1E-03 = 1\ kg\ m^{-3}$
$1\ cm \times 1E+02 = 1\ m$

provides a more accurate prediction of fracture temperature profile applicable for acid fracturing of limestone reservoirs.

2. Modeling and computational methods

2.1. Calculation of acid–rock molar reaction heat

Limestone is mainly composed of calcium carbonate. During acid fracturing, hydrochloric acid quickly reacts with limestone according to the following ionic reaction equation:

$$CaCO_3 + 2H^+ = Ca^{2+} + H_2O + CO_2\uparrow \quad (1)$$

The molar reaction enthalpy of reaction at 298.15 K is $\Delta_r H_m^\Theta$. $\Delta_r H_m^\Theta$ is calculated by standard molar formation enthalpies $\Delta_f H_m^\Theta$, values of which can be obtained from the Handbook of Physical Chemistry (Perry and Green, 1997).

The temperatures of acid–rock reactions in the fractures are usually much higher than the normal surface temperatures in carbonate reservoirs. According to Kirchhoff's law, the standard molar reaction enthalpies of $CaCO_3$ and H^+ at fracture surface can be expressed as

$$\Delta_r H_m^\Theta(T_w) = \Delta_r H_m^\Theta(298.15\ K) + \int_{298.15\ K}^{T_w} [C_{p,m}(Ca^{2+}, T) + C_{p,m}(H_2O, T) + C_{p,m}(CO_2, T) - C_{p,m}(CaCO_3, T) - 2C_{p,m}(H^+, T)]dT \quad (2)$$

where T_w represents the temperature at fracture surface with unit K, and $C_{p,m}$ is the constant-pressure molar heat capacity with unit $J\ K^{-1}\ mol^{-1}$, which is a function of temperature and the correlation can usually be expressed as $C_{p,m} = a + bT + cT^2 + \ldots\ldots$ or $C_{p,m} = a + bT + (c'/T^2) + \ldots\ldots$. For the matters in Eq. (2), each related parameters is specified in Table 1.

Substitute values of Table 1 into Eq. (2), and solve the integration, then we get the expression of $\Delta_r H_m^\Theta(T_w)$ as follows:

$$\Delta_r H_m^\Theta(T_w) = -13.692 + \frac{1}{1000}\left(-6.443 \times 10^{-3} T_w^2 + 16.075 T_w - \frac{17.406 \times 10^5}{T_w}\right) \quad (3)$$

During acid fracturing, the pressure in the fracture is tens of MPa, which will also make the molar reaction enthalpies different from those standard states. According to the Second Law of

Table 1
Thermodynamic data for parameters in Eq. (2).

	$\Delta_f H_m^\Theta$	$C_{p,m}(T) = a + bT + c'T^{-2}$		
	($kJ\ mol^{-1}$)	a ($J\ K^{-1}\ mol^{-1}$)	b ($10^{-3} J\ K^{-2}\ mol^{-1}$)	c' ($10^5 J\ K\ mol^{-1}$)
Ca^{2+} (aq)	−542.83	0.97	0	0
H_2O (l)	−285.84	75.48	0	0
CO_2 (g)	−393.51	44.141	9.037	−8.535
$CaCO_3$ (s)	−1206.87	104.516	21.924	−25.941
H^+ (aq)	0		0	

Thermodynamics, the relationship between molar reaction enthalpy and pressure is given by the equation (Han and Gao, 1997)

$$\Delta_r H_m(T,p)=\Delta_r H_m^{\Theta}(T)+1000\int_{1\ \mathrm{atm}}^{p}\sum_i \nu_i\left(V_i-T\left(\frac{\partial V_i}{\partial T}\right)_p\right)_T dp \tag{4}$$

where ν_i is the stoichiometric coefficient of substance i in the chemical reaction equation and V_i is molar volume of i, with unit $m^3\ mol^{-1}$. In the reaction between calcium carbonate and hydrochloric acid, all the reactants and products, except for the undissolved CO_2, are in a condensed state. The thermal cubic expansion coefficients of condensed matters are all comparably smaller than those of gases. So $V_c-T_w(\partial V_c/\partial T)_p\approx V_c$ is assumed (Han and Gao, 1997), where the subscript c denotes condensed matters. The volume of the aqueous system hardly changes during reaction, so we consider $\sum_c \nu_c(V_c)_{T_w,p}\approx 0$. Therefore, the pressure of the system mainly comes from gaseous CO_2, and Eq. (4) can be changed into

$$\Delta_r H_m(T_w,p)=\Delta_r H_m^{\Theta}(T_w)+1000 f_g\int_{0.101}^{p}\left(V_{CO_2}-T_w\left(\frac{\partial V_{CO_2}}{\partial T}\right)_p\right)_{T_w} dp \tag{5}$$

where p is pressure, in units MPa; V_{CO_2} is molar volume of CO_2, $m^3\ mol^{-1}$, which is a function of temperature and pressure. In this paper, BWR state equation (Xue et al., 2004) was selected to calculate the molar volume V_{CO_2}. The reason is that the critical pressure and temperature of CO_2 is 7.4 MPa and 31 °C, respectively. Both the pressure and temperature in carbonate reservoirs are usually higher than the critical state of CO_2. So the gaseous CO_2 in hydraulic fracture is in its supercritical state. Until now, there are 100 state equations available in the literature. Among them, the BWR state equation with eight empirical parameters is widely used to describe the supercritical state of CO_2 (Benedict et al., 1940; Xue et al., 2004). As a result, it was selected to calculate the molar volume V_{CO_2} in Eq. (5). The calculation process can be seen from reference Huang et al. (2009).

Another parameter f_g in Eq. (5) is the molar fraction of free CO_2, which is also the ratio of the amount of free CO_2 to the total amount of CO_2 generated when 1 mol reaction occurs. f_g can be calculated by the following expression:

$$f_g=1-\frac{V_{acid}S_{CO_2}}{22.4} \tag{6}$$

where V_{acid} is the volume of the reacted acid when 1 mol of CO_2 is generated in the reaction, in units liters; S_{CO_2} is the solubility of carbon dioxide in the reacted acid at certain temperature and pressure, $m^3\ m^{-3}$.

Since gaseous CO_2 is produced in the reaction of calcium carbonate and hydrochloride acid, this reaction is referred to as an expanding process, during which the reaction system does volumetric work to its environment. But only a portion of the reaction enthalpies is released in the form of heat. When 1 mol reaction occurs, the actual heat effect is given by (Fu et al., 1990)

$$\Delta_r Q_m(T_w,\ p)=\Delta_r H_m(T_w,\ p)-[-p(f_g V_{CO_2})] \tag{7}$$

where $\Delta_r Q_m(T_w,\ p)$ is the molar reaction heat of reacting calcium carbonate and hydrochloric acid. Substituting Eqs. (3) and (5) into Eq. (7), the actual molar reaction heat can be expressed as

$$\begin{aligned}\Delta_r Q_m(T_w,\ p)=&-13.692+\tfrac{1}{1000}\Big(-6.443\times10^{-3}T_w{}^2\\&+16.075T_w-\frac{17.406\times10^5}{T_w}\Big)\\&+f_g\int_{1atm}^{p}\left[V_{CO_2}-T_w\left(\frac{\partial V_{CO_2}}{\partial T}\right)_p\right]_{T_w}dp+pf_gV_{CO_2}.\end{aligned} \tag{8}$$

2.2. Coupling of acid–rock reaction heat and temperature profile model

A large portion of fluid is usually lost during acid fracturing of carbonate formations through the wormholes. Nevertheless, this paper mainly focuses on the effects of acid–rock reaction heat on fluid temperature, paying little attention to the modeling of fracture propagation. Therefore, the analytical solution considering fluid loss (Nordgren, 1972) has been employed to describe the geometry of fracture, fracture length is given by

$$L(t)=\frac{Q_i t^{1/2}}{2\pi Ch} \tag{9}$$

while fracture width could be calculated by

$$w(x,\ t)=w(0,\ t)\left[\left(\frac{x}{L(t)}\right)\sin^{-1}\left(\frac{x}{L(t)}\right)+\sqrt{1-\left(\frac{x}{L(t)}\right)^2}-\frac{\pi}{2}\left(\frac{x}{L(t)}\right)\right]^{1/4} \tag{10}$$

where

$$w(0,\ t)=\frac{1.425\pi}{4}\left[\frac{2(1-\nu^2)\mu_f Q_i^2}{ECh}\right]^{1/4}t^{1/8}. \tag{11}$$

In Eqs. (9)–(11), L is the fracture length, m; w is the average fracture width along the fracture height, m; Q_i is the injection rate, $m^3\ min^{-1}$; t is time, min; E is the Young's modulus, MPa; C is the leak-off coefficient of acid, $m\ min^{-0.5}$; h is the thickness of the formation, m; ν is the Poisson's ratio; μ_f is the fluid viscosity, mPa s; x is the distance from wellbore, m.

The model of acid flow in a fracture is illustrated in Fig. 1. The energy conservation equation for the fluid can be expressed as (Whitsitt and Dysart, 1970)

$$\frac{\partial(v_x T)}{\partial x}+\frac{\partial(v_y T)}{\partial y}=\frac{K_{hf}}{\rho_f C_f}\frac{\partial^2 T}{\partial y^2} \tag{12}$$

with boundary conditions

$$x=0,\quad T=T_0 \tag{13}$$

$$y=0,\quad \frac{\partial T}{\partial y}=0 \tag{14}$$

and

$$y=\pm\frac{w}{2},\quad K_{hf}\frac{\partial T}{\partial y}=k_R C_A{}^m[-\Delta_r Q_m(T_w,\ p)]+q_h(t) \tag{15}$$

where $\Delta_r Q_m(T_w,p)$ is the acid–rock reaction heat as expressed by Eq. (8); K_{hf} is the thermal conductivity of fracture fluid; ρ_f and C_f

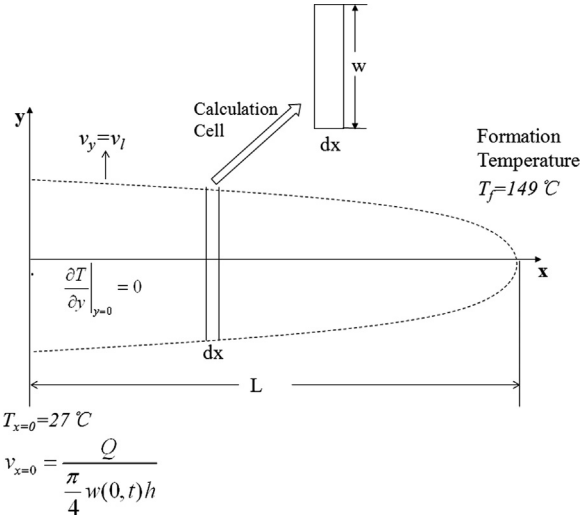

Fig. 1. Illustration of acid flow in a fracture.

denote the density and the specific heat of fracture fluid, respectively; k_R is the reaction rate constant, which is a function of temperature; m is the order of reaction; C_A is the acid concentration; $q_h(t)$ is the heat flux from the formation to fracture, which can be expressed by the analytical equation derived by Whitsitt and Dysart (1970):

$$q_h(t)=\sqrt{\frac{M_{ma}K_{hr}}{\pi t}}(T_i-T_w)\left[e^{-\zeta^2}-\sqrt{\pi}\zeta erfc(\zeta)\right] \tag{16}$$

where

$$\zeta=\frac{v_l C_f\rho_f}{2(1-\varphi)}\sqrt{\frac{t}{M_{ma}K_{hr}}} \tag{17}$$

v_x and $v_y$represent the flow velocity of acid in the direction of fracture length and width respectively, which satisfy the equation of continuity (Roberts and Guin, 1975)

$$\frac{\partial v_x}{\partial x}+\frac{\partial v_y}{\partial y}=0 \tag{18}$$

with the boundary conditions

$$x=0,\quad v=\frac{Q_i}{(\pi/4)w(0,\ t)h} \tag{19}$$

$$y=\pm\frac{w}{2},\quad v_y=v_l \tag{20}$$

and the acid concentration C_A meets the mass balance equation

$$\frac{\partial(v_xC_A)}{\partial x}+\frac{\partial(v_yC_A)}{\partial y}=\frac{\partial}{\partial y}\left(D_e\frac{\partial C_A}{\partial y}\right) \tag{21}$$

with the boundary conditions

$$x=0,\quad C_A=C_{A0} \tag{22}$$

$$y=0\quad \frac{\partial C_A}{\partial y}=0 \tag{23}$$

$$y=\pm\frac{w}{2},\quad -D_e\frac{\partial C_A}{\partial y}=k_RC_A^m \tag{24}$$

Eqs. (12), (18) and (21) can be transformed into ordinary equations using lumping procedures:

$$w\overline{v_x}\frac{d\overline{T}}{dx}=2\left(v_l-\frac{h_T}{\rho_fC_f}\right)(\overline{T}-T_w) \tag{25}$$

$$\frac{w}{2}\frac{d\overline{v_x}}{dx}+v_l=0 \tag{26}$$

$$w\overline{v_x}\frac{d\overline{C_A}}{dx}=2(v_l-k_g)(\overline{C_A}-C_w) \tag{27}$$

where $\overline{T}$, $\overline{v_x}$and $\overline{C}$ are the average values of acid temperature, flow velocity and acid concentration, respectively, in the direction of the fracture width. v_l is the leak off velocity. T_w and C_w are the temperature and acid concentration at fracture surface respectively, which can be calculated from the following equations:

$$h_T(T_w-\overline{T})=k_R{C_w}^m[-\Delta_rQ_m(T_w,\ p)]+q_h(t) \tag{28}$$

$$k_g(\overline{C}-C_w)=k_R{C_w}^m \tag{29}$$

h_T and k_g in Eqs. (25) and (27) are respectively the heat transfer coefficient and the mass transfer coefficient at specific fracture segment, which can be calculated using the method presented in Mou et al. (2010).

$\Delta_rQ_m(T_w,\ p)$ is also a function of pressure, so the pressure profile in fracture should be calculated as well. According to the theory of elastic mechanics (Cleary et al., 1983), the net pressure in fracture is proportional to the dynamic fracture width,

$$\Delta p=p-p_c=\frac{2E}{\pi(1-\nu^2)h}w(x,\ t) \tag{30}$$

Then the real pressure in fracture segment i is

$$p_i=p_c+\frac{2E}{\pi(1-\nu^2)h}w_i \tag{31}$$

where p_c is the closure pressure with unit MPa.

Starting from the fracture inlet, and solving the equations for each fracture segment, the solution of the former segment is the boundary condition of the last segment. The ordinary differential Eqs. (25)–(27) can be solved using Runge–Kutta method. Eqs. (28) and (29) can be solved by Newton–Raphson method and the average fluid temperature $\overline{T}$ in each fracture segment can be obtained consequently. The detailed solving procedures are as follows: (1) calculate dynamic fracture length L and width w_i at $n=1$ according to Eqs. (9)–(11); (2) calculate the acid velocity distribution and the pressure profile at the same time interval; (3) enter the initial concentration and temperature of acid at $i=0$ (fracture inlet), C_0 and T_0, as input data; (4) calculate the mass transfer coefficient k_g, heat transfer coefficient h_T and acid–rock reaction constant k_R at the first fracture segment; (5) calculate acid concentration at the fracture surface $C_w(i)$ using the binary divisive procedure; (6) calculate the temperature at the fracture surface $T_w(i)$ using Newton iteration method, and acid–rock reaction heat $\Delta_rQ_m(T_w,\ p)$ can be obtained simultaneously; (7) solve Eqs. (25) and (27) using Runge–Kutta method, and the average acid concentration $\overline{C}$ and the average temperature $\overline{T}$ at the next fracture segment ($i=i+1$) can be obtained; (8) judge: if i is the last fracture segment, stop and go to step (9); else go to step (4) to calculate the next fracture segment; and (9) judge: if pumping terminates, then end the calculation; else go to step (1) to calculate the next time interval.

3. Discussion of computational results

3.1. Acid–rock reaction heat

A series of programs have been developed to calculate the fluid temperature profiles, based on the influence of the acid–rock reaction heat. Table 2 shows the basic input data that has been used in this study to calculate the fluid temperature profile in a fracture during acid fracturing of a carbonate reservoir. The effect of acid–rock reaction heat at pump-off time has been considered in the evaluation of the fluid temperature profiles.

Fig. 2 illustrates the comparison of the fluid temperature profiles along the acid-fracture during pump-off time for the conditions, with and without the effects of acid–rock reaction heat. The horizontal axis is a dimensionless distance which is the ratio of distance x and fracture length L. The curves show that the fluid temperatures will be significantly higher in the distance from 10% to 70% of fracture length when acid–rock reaction heat is taken into consideration. At the same time, the two curves will overlap at the distance close to and far from the wellbore. This is because there is always a steady supply of cold acid at the fracture inlet (close to wellbore), simultaneously replacing the heated acid. Close to the end of the fracture (far from the wellbore), however, the concentration of acid has become very low, leading to a weak reaction with little or no heat generation.

Fig. 3 shows the variation of fluid temperature increments solely caused by the acid–rock reaction in the fracture. The curve indicates that the temperature increment rises rapidly to 13 °C in the first third of the fracture length from the wellbore, and then gradually declines to zero toward the end of the fracture. However,

Table 2
Input data for calculating fluid temperature profile in fracture.

Category	Parameter	Value
Formation data	Bed thickness, m	15.24
	Porosity, %	8.00
	Initial formation temperature, °C	149.00
	Closure stress, MPa	70.00
Construction data	Acid volume, m^3	151.40
	Pump rate, $m^3\ min^{-1}$	1.59
Acid property data	Acid strength, %	28.00
	Acid viscosity, mPa s	10.00
	Specific heat of acid, $J\ kg^{-1}\ °C^{-1}$	4182.00
	Thermal conductivity of acid, $W\ m^{-1}\ °C^{-1}$	0.55
	Effective H^+ diffusion coefficient at 25 °C, $cm^2\ s^{-1}$	5.00E−05
	Acid leak off coefficient, $m\ min^{-0.5}$	6.00E−04
Rock property data	Rock type	Limestone
	Rock density, $g\ cm^{-3}$	2.60
	Young's modulus, MPa	27,580.00
	Poisson's ratio, dimensionless	0.30
	Specific heat of rock, $J\ kg^{-1}\ °C^{-1}$	880.00
	Thermal conductivity of rock, $W\ m^{-1}\ °C^{-1}$	1.57
Reaction kinetics data	Activation energy, $J\ mol^{-1}$	12,354.00
	Frequency factor, $10^{3m} mol^{1-m}\ cm^{3m-2}\ s^{-1}$	1.65E−03
	Order of reaction	0.44

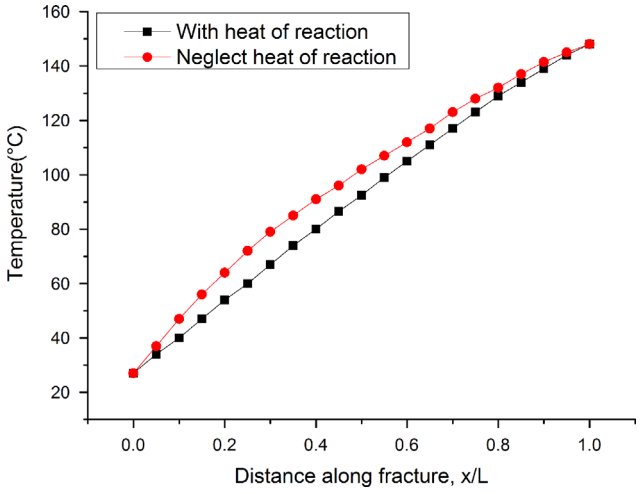

Fig. 2. Effects of acid–rock reaction heat on fluid temperature profile.

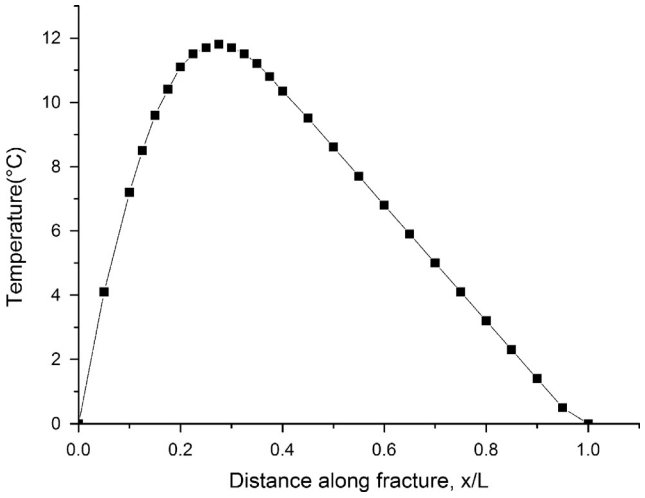

Fig. 3. Fluid temperature increments solely caused by the acid–rock reaction in the fracture.

Lee and Roberts (1980) observed a fluid temperature increase of 40 °C by similar input data, assuming a constant acid–molar reaction heat. This difference indicates that if we treat the reaction heat as a constant, the predicted temperature will be higher.

Figs. 4 and 5, and Table 3, respectively, illustrate the effects of temperature, pressure and volumetric work of CO_2 on acid–rock molar reaction heat. Generally, at any given pressure, a change in fluid temperature by 20 °C will cause the molar reaction heat to vary in the range of 1–5 $kJ\ mol^{-1}$. Furthermore, changing the pressure by 5 MPa will cause the molar reaction heat to vary in the range of 0.5–1 $kJ\ mol^{-1}$ at constant temperature, see Figs. 4 and 5. In Fig. 5, the reaction heat decreases when the pressure is lower than 30 MPa, but increases when pressure is higher. When the pressure is relatively low, attractive force plays a predominant role between the molecules. With the increase of pressure, the distance between the molecules decreases and attractive potential energy increases. The increase of attractive potential energy will cause a decrease in the thermodynamic energy. As a result, the temperature of the system would drop. While the pressure is relatively high, repulsive force plays a predominant role between the molecules. With the increase of pressure, the increase of repulsive potential energy will also cause an increase in the thermodynamic energy. As a result, the temperature of the system would increase. Therefore, when attractive and repulsive forces are balanced at certain pressure, thermodynamic energy reduces to the minimum and the temperature shows the lowest value. Table 3 shows the effects of volumetric work on acid–rock molar reaction heat. Keeping the fluid temperature and pressure at 150 °C and 80 MPa, respectively, raising the acid concentration from 10% to 28%, neglecting the effect of volumetric work, an error as big as 25% for the calculation of molar reaction heat may occur. Therefore, it is of great importance to consider the effects of temperature, pressure and volumetric work of CO_2 in the prediction of acid–rock molar reaction heat.

3.2. *Effects of acid–rock reaction heat on temperature profile*

In order to examine the effects of acid–rock reaction heat on temperature profile under different acid concentrations, three acid concentrations, 15%, 18% and 24%, were separately reacted with limestone (from Shengli oil field). Table 4 shows the reaction

kinetics parameters measured by experiments. The frequency factor and the activation energy change with the consumption of the acid. However, the values recorded in Table 4 and used in our model input data are average values. Other input data for this model are drawn from Table 2. The calculation results show that at any point along the fracture, the temperature increase caused by reaction heat will be the highest for the fluid with the highest acid concentration and correspondingly lower for low acid concentrations as shown in Fig. 6. This is because the reaction rate and heat is proportional to the acid concentration. Moreover, it takes a little longer for an acid with a higher concentration to become inactive, resulting in a longer time for the generated reaction heat to warm the fluid.

By changing the initial formation temperature in Table 2, the effects of acid–rock reaction heat on temperature profile at different formation temperatures can be evaluated. Three temperature values, 120 °C, 150 °C, 180 °C were selected to illustrate the difference. The fluid temperature profiles vary significantly at different initial formation temperatures, so it is meaningless to compare the values of the temperature increments. Therefore, the concept of percent of temperature increase is introduced, which is defined as the ratio of the temperature increase caused by the reaction heat to the actual fluid temperature. In other words, this is the relative error caused by neglecting the reaction heat. Fig. 7 depicts percent of temperature increase along the fracture under different initial formation temperatures. The curves indicate that errors as big as 19% can be caused when acid–rock reaction heat is neglected. It is also to be observed

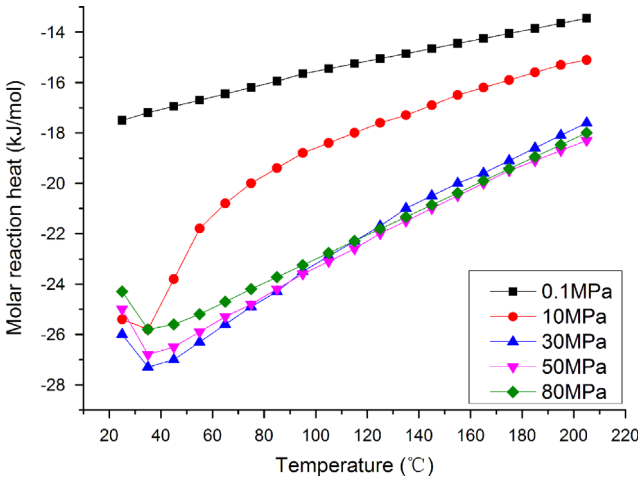

Fig. 4. Effects of temperature on acid–rock molar reaction heat.

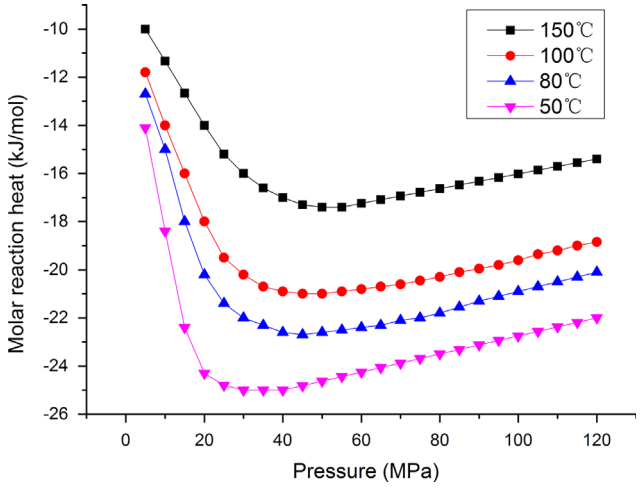

Fig. 5. Effects of pressure on acid–rock molar reaction heat.

Table 4
Reaction kinetics parameters of Shengli limestones with different HCl concentrations.

Acid concentration (%)	Frequency factor (10^{3m} mol^{1-m} cm^{3m-2} s^{-1})	Activity energy (J mol^{-1})	Order of reaction
15	1.81E−03	13,786.40	0.73
18	3.43E−03	16,853.50	1.23
24	1.24E−02	22,234.90	1.30

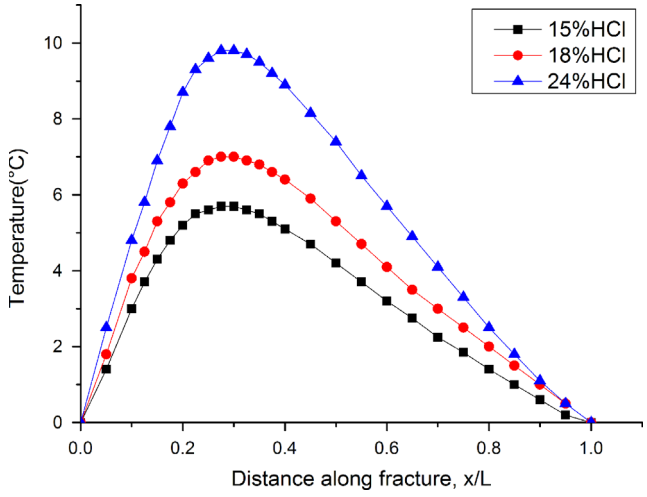

Fig. 6. Effects of acid concentration on fluid temperature profile.

Table 3
Effects of volumetric work on acid–rock molar reaction heat.

Temperature (°C)	Pressure (MPa)	Acid concentration (%)	Molar reaction heat (kJ mol)		Errors caused by neglect of volumetric work (%)
			With volumetric work	Without volumetric work	
60	30	10	−18.20	−18.93	4.04
60	30	20	−21.49	−22.85	6.30
60	30	28	−22.25	−23.74	6.72
100	50	10	−14.44	−14.93	3.39
100	50	20	−18.59	−20.79	11.83
100	50	28	−19.23	−21.70	12.81
150	80	10	−12.16	−12.16	0.00
150	80	20	−14.81	−18.05	21.91
150	80	28	−15.26	−19.05	24.88

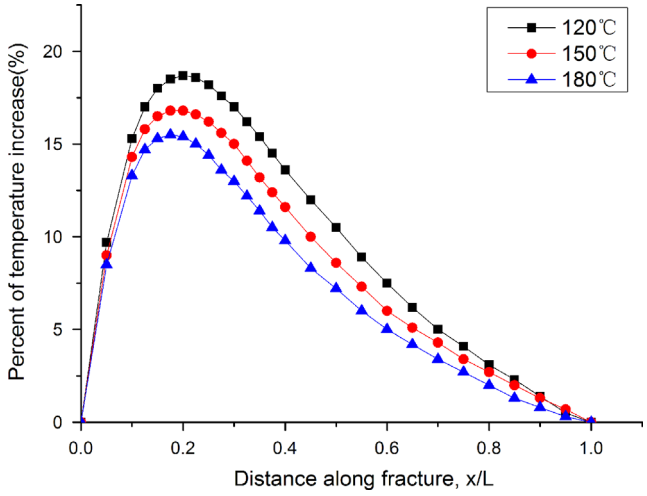

Fig. 7. Effect of reaction heat on temperature profile in fracture at different initial formation temperatures.

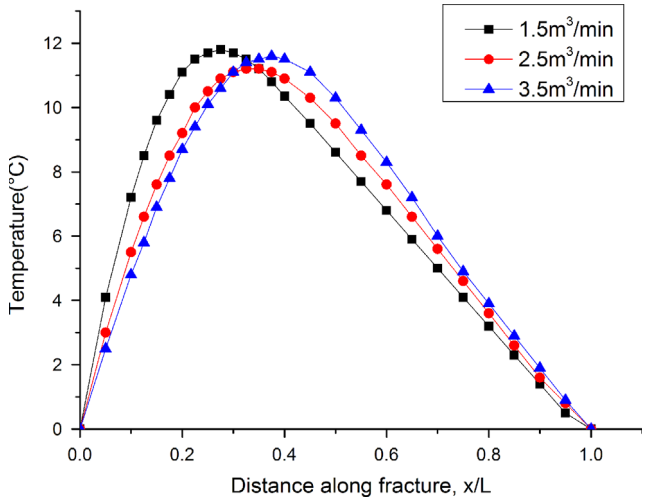

Fig. 8. Effects of acid–rock reaction heat on temperature profiles at different pump rates.

that the lower the initial formation temperature, the more pronounced effect of the acid–rock reaction heat on the fluid temperature profile. Therefore, for the accurate calculation of acid–rock reaction heat, much attention is required when acid fracturing modeling is done in low-temperature formations.

Similarly, the effects of reaction heat on temperature profiles at different pump rate can be examined by changing the value of the pump rate in Table 2. Three pump rates, 1.5, 2.5 and 3.5 $m^3\ min^{-1}$ were chosen, while the other input data remain the same. The calculation results are shown in Fig. 8. It can be seen from the curves that there is no specific correlation between the temperature increments along the fracture profile, as caused by the acid–rock reaction heat at the different pump rates. However, the higher the pump-rate is, the farther the position of the highest temperature will be. This is because the larger the pump rate, the higher the flow velocity of the fluid, and the more intense the heat convection in the direction of the fracture length, so that heat is more easily transported in the direction of fluid flow.

4. Conclusions

According to the calculation and discussion, the following conclusions could be summarized: (1) acid–rock reaction heat can cause a maximum temperature increase of 15 °C in the fracture fluid; (2) the effects of acid–rock reaction heat on the fluid temperature profile become more important with increased acid concentration and decreased initial formation temperature; and (3) it is important to consider the effects of temperature, pressure and volumetric work of CO_2 in the prediction of acid–rock molar reaction heat, which in turn makes the calculation of the temperature profile more accurate.

Acknowledgment

Financial support from the National Natural Science Foundation of China (Grant no. 51074138) is gratefully acknowledged.

References

Benedict, M., Webb, G.B., Rubin, L.C., 1940. An empirical equation for thermodynamic properties of light hydrocarbons and their mixtures I. Methane, ethane, propane and n-butane. J. Chem. Phys. 8 (4), 334.
Cleary, M.P., Keek, R.G., Mear, M.E., 1983. Microcomputer models for the design of hydraulic fractures. In: Paper SPE 11628, Presented at the SPE/DOE Low Permeability Gas Reservoirs Symposium, Denver, Colorado, 14–16 March.
Dysart, G.R., Whitsitt, N.F., 1967. Fluid temperature in fractures. In: Paper SPE 1902, Presented at the Fall Meeting of the Society of Petroleum Engineers of AIME, New Orleans, Louisiana, 1–4 October.
Fu, X.C., Shen, W.X., Yao, T.Y., 1990. Physical Chemistry, 4th edition Higher Education Press, Beijing, China (in Chinese).
Hasan, A.R., Kabir, C.S., 1994. Aspects of wellbore heat transfer during two-phase flow (includes associated papers 30226 and 30970. Old Prod. Facil. 9 (3), 211–216.
Han, D.G., Gao, Z.D., 1997. Chemical Thermodynamics. Higher Education Press, Beijing, China (in Chinese).
Huang, W.S., Hu, Y.Q., Zhao, J.Z., 2009. Pseudo three dimension acid fracturing pressure decline curve analysis model. Fault-Block Oil Gas Field 16 (1), 75–77 (in Chinese).
Lee, M.H., Roberts, L.D., 1980. Effect of heat of reaction on temperature distribution and acid penetration in a fracture. Old SPE J. 20 (6), 501–507.
Medeiros Jr., F., Trevisan, O.V., 2006. Thermal analysis in matrix acidization. J. Pet. Sci. Eng. 51 (1), 85–96.
Mou, J.Y., Zhu, D., Hill, A.D., 2010. A new acid-fracture conductivity model based on the spatial distributions of formation properties. In: Paper SPE 127935, Presented at SPE International Symposium and Exhibition on Formation Damage Control, Lafayette, Louisiana, 10–12 February.
Nordgren, R.P., 1972. Propagation of a vertical hydraulic fracture. SPE J. 12 (4), 306–314.
Perry, R.H., Green, D., 1997. Chemical Engineers Handbook, 7th edition McGraw Hill Professional, London.
Roberts, L.D., Guin, L.A., 1975. A new method for predicting acid penetration distance. Old SPE J. 15 (4), 277–286.
Ren, S.Q., Xiong, H.J., 1989. Temperature and common ion effects on effective acid penetration in a fracture. SPE Prod. Eng. 4 (3), 221–225.
Roodhart, L.P., Koninklijike, K.H., Davies, D.R., 1993. Improved acid fracturing treatment designs based on in-situ temperature calculations. In: Paper SPE 26185, Presented at the SPE Gas Technology Symposium, Calgary, Alberta, Canada, 28–30 June.
Settari, A., 1993. Modeling of acid-fracturing treatments. Old Prod. Facil. 8 (1), 30–38.
Squier, D.P., Smith, D.D., Dougherty, E.L., 1962. Calculated temperature behavior of hot-water injection wells. J. Pet. Technol. 14 (4), 436–440.
Whitsitt, N.F., Dysart, G.R., 1970. The effect of temperature on stimulation design. J. Pet. Technol. 22 (4), 493–502.
Wu, Y.S., Pruess, K., 1990. An analytical solution for wellbore heat transmission in layered formations (includes associated papers 23410 and 23411. SPE Reserv. Eng. 5 (4), 531–538.
Xue, W.D., Zhu, Z.H., Zou, L.X., Zhang, G.F., 2004. Theoretic calculation on thermodynamic character for SCF CO_2. J. At. Mol. Phys. 21 (2), 295–300 (in Chinese).
Zhu, D., Hill, A.D., 1991. The effect of temperature on minifrac pressure decline. In: Paper SPE 22874, Presented at the SPE Annual Technical Conference and Exhibition, Dallas, Texas, 6–9 October.